

16. DATA REPORT: HIGH-RESOLUTION INORGANIC GEOCHEMISTRY ACROSS THE PALEOCENE/EOCENE BOUNDARY, HOLE 1221C¹

Peter A. Knoop²

ABSTRACT

A record of inorganic geochemical variability was produced from a contiguous sequence of 35 samples, with 1 cm spacing, recovered from Hole 1221C. This record covers from 153.91 to 154.27 meters below seafloor and spans the Carbon Isotope Excursion (CIE) associated with the Paleocene/Eocene boundary interval. Elemental concentrations were determined for Al, As, Ba, Ca, Fe, K, Mg, Mn, P, Si, Sr, Ti, Cd, Co, Cr, Cu, Hf, Mo, Nb, Ni, Pb, Pt, Re, Sc, V, Y, Zn, La, Ce, Pr, Nd, Pm, Sm, Eu, Gd, Tb, Dy, Ho, Er, Tm, Yb, and Lu. Most concentration profiles exhibit a marked peak coincident with or just prior to the CIE. In addition, the rare earth element pattern exhibits a significant flattening of the typical, prominent negative Ce anomaly across the same interval.

INTRODUCTION

The Paleocene/Eocene (P/E) boundary is a period of substantial warming (~5°–7°C) in surface and deep ocean waters, extinction of 35%–50% of deep-sea benthic foraminifers, rapid perturbation to the global geochemical carbon cycle, and significant changes in Northern Hemisphere terrestrial fauna (e.g., Kennett and Stott, 1991; Zachos et al., 1993; Koch et al., 1992; Gingerich, 2000). These events are believed to have occurred over a very short time period; in particular, high-resolution stable isotope records suggest that the carbon cycle was per-

¹Knoop, P.A., 2005. Data report: High-resolution inorganic geochemistry across the Paleocene/Eocene boundary, Hole 1221C. In Wilson, P.A., Lyle, M., and Firth, J.V. (Eds.), *Proc. ODP, Sci. Results*, 199, 1–12 [Online]. Available from World Wide Web: <http://www-odp.tamu.edu/publications/199_SR/VOLUME/CHAPTERS/220.PDF>. [Cited YYYY-MM-DD]

²University of Michigan, School of Information, 1075 Beal Avenue, Ann Arbor MI 48109-2112, USA.
knoop@umich.edu

turbed extremely rapidly, on a scale of less than a single ~26-k.y. precession cycle (e.g., Bains et al., 1999; Norris and Röhl, 1999). It has been suggested that a possible cause for these events is the massive release and oxidation of methane from marine gas hydrate reservoirs (e.g., Dickens et al., 1997; Katz et al., 1999). Such an event would be expected to influence the bulk geochemistry of sediments through changes in dissolved oxygen and chemical inputs to the ocean.

Another possible driver for changes in bulk geochemistry across this interval is increased hydrothermal sedimentation. An increase in hydrothermal sediment fluxes associated with plate boundary reorganization at the P/E boundary has been previously documented (Rea et al., 1990). The age of the lowermost chalks (56.5–57 Ma) suggests that Site 1221 was in relatively close proximity to the paleo-ridge-crest at the time of P/E deposition and could preserve a record of such variability.

The sediments recovered during Leg 199 can help us to further evaluate such hypotheses by filling important gaps in our knowledge of this critical time interval, as few P/E sections have been recovered in the Pacific. The P/E interval was recovered from Holes 1220B, 1221C, and 1221D, all of which exhibit a dramatic yet similar visual appearance across this interval (see figure F30 in Shipboard Scientific Party, 2002). The data generated in this study represent one of the very first high-resolution records of bulk geochemistry across the marine P/E boundary.

METHODS

Samples were fully digested for analysis using a sodium peroxide technique, modified from Sulcek and Povondra (1989), Kleinhanns et al. (2002), and Meisel et al. (2002). Approximately 0.05 g of sample was well-mixed with ~0.95 g of sodium peroxide in a zirconium crucible and heated in a 500°C oven for 30 min. The sodium peroxide was ground to a fine powder using mortar and pestle prior to use in order to maximize surface area and minimize interaction with atmospheric moisture.

After removal from the oven and cooling to room temperature, 5 mL of concentrated quartz-distilled HNO₃ was slowly added dropwise to the solid residue in the crucible. The resulting solution and remaining solid residue were washed with triple-distilled water into a 30 mL polyethylene (LDPE) bottle. Three drops of concentrated quartz-distilled HCl and 80 µL of ultra-pure hydrogen peroxide were added to dissolve the remaining residue, which was suspected to be iron and manganese compounds.

Finally, each solution was brought up to a uniform volume of ~30 mL using triple-distilled water. The exact initial sample mass and sample solution mass were recorded and used to correct the analytical results in determining actual elemental concentrations. Further corrections were applied to account for dilutions necessary to bring elemental concentrations into appropriate ranges for analyses.

Elemental analyses were carried out by inductively coupled plasma-optical emission spectrometer (ICP-OES) on a Perkin-Elmer Optima 3300DV, except for the rare earth elements (REEs), which were analyzed by ICP-mass spectroscopy (MS) on a Finnegan Element mass spectrometer. La, Ce, and Ba were analyzed using both techniques as a crosscheck, though at different dilution levels.

RESULTS AND SUMMARY

The inorganic geochemical record produced in this study covers 153.91 to 154.27 meters below seafloor (mbsf) in Hole 1221C. This depth interval includes the $\delta^{13}\text{C}$ excursion associated with the P/E boundary (Fig. F1).

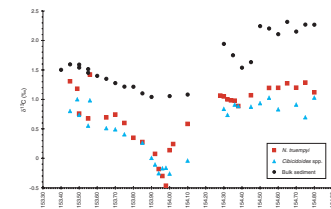
Elemental concentrations were determined for Al, Ba, Ca, Fe, K, Mg, Mn, P, Si, Sr, Ti, Cd, Co, Cr, Cu, Hf, Mo, Nb, Ni, Pb, Sc, Sb, Se, Sn, V, Y, Zn, As, Pd, La, Ce, Pr, Nd, Pm, Sm, Eu, Gd, Tb, Dy, Ho, Er, Tm, Yb, Lu, Re, Os, Ir, and Pt on 35 samples (Tables T1, T2). When plotted against depth, most concentration profiles reveal significant changes across the boundary interval (Fig. F2). A correlation analysis of the concentration data (Table T3) highlights elements exhibiting similar depth-dependent variability.

Post-Archean Australian Shale (PAAS)-normalized REE patterns were calculated for each sample (Fig. F3). The majority of the samples exhibit a similar pattern, with a prominent negative Ce anomaly. Samples in the vicinity of other rapidly changing elemental concentrations, however, have a much flatter Ce anomaly in the interval 154.11–154.17 mbsf.

ACKNOWLEDGMENTS

The samples analyzed in this report were collected shipboard during Leg 199 by the author with the assistance of Dick Norris and Paula Weiss. Sample preparation and elemental analyses were carried out in the Radiogenic Isotope Geochemistry Laboratory, Department of Geological Sciences, University of Michigan, USA, except for REE analyses, which were conducted in the Keck Elemental Geochemistry Laboratory, Department of Geological Sciences, University of Michigan, USA. Analytical assistance was provided by Ted Huston and Andrea Klaue. This research used samples and/or data provided by the Ocean Drilling Program (ODP). ODP is sponsored by the U.S. National Science Foundation (NSF) and participating countries under management of Joint Oceanographic Institutions (JOI), Inc. Funding for this effort was provided by the JOI/United States Science Support Program (USSSP).

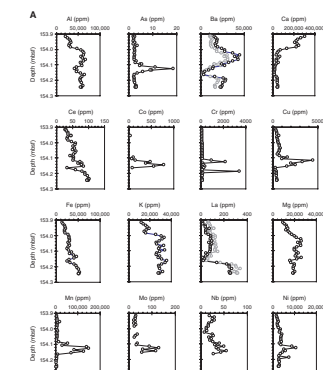
F1. Carbon isotope values, p. 5.



T1. ICP-OES elemental concentrations, p. 9.

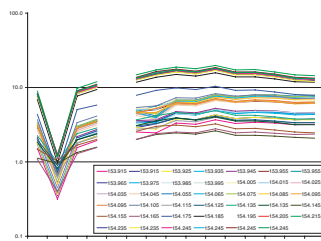
T2. ICP-MS elemental concentrations, p. 11.

F2. Elemental concentration profiles, p. 6



T3. Elemental data correlation, p. 12.

F3. REE patterns, p. 8.



REFERENCES

- Bains, S., Corfield, R.M., and Norris, R.D., 1999. Mechanisms of climate warming at the end of the Paleocene. *Science*, 285:724–727.
- Dickens, G.R., Castillo, M.M., and Walker, J.G.C., 1997. A blast of gas in the latest Paleocene: simulating first-order effects of massive dissociation of oceanic methane hydrate. *Geology*, 25(3):259–262.
- Gingerich, P.D., 2000. Paleocene/Eocene boundary and continental vertebrate faunas of Europe and North America. *GGF*, 122(1):57–59.
- Katz, M.E., Pak, D.K., Dickens, G.R., and Miller, K.G., 1999. The source and fate of massive carbon input during the latest Paleocene thermal maximum. *Science*, 286:1531–1533.
- Kennett, J.P., and Stott, L.D., 1991. Abrupt deep-sea warming, paleoceanographic changes and benthic extinctions at the end of the Palaeocene. *Nature*, 353:225–229.
- Kleinhanns, I.C., Kreissig, K., Kamber, B.S., Meisel, T., Nagler, T.F., and Kramers, J.D., 2002. Combined chemical separation of Lu, Hf, Sm, Nd and REEs from a single rock digest: precise and accurate isotope determination of Lu-Hf and Sm-Nd using multicollector-ICPMS. *Anal. Chem.*, 74:67–73.
- Koch, P.L., Zachos, J.C., and Gingerich, P.D., 1992. Correlation between isotope records in marine and continental carbon reservoirs near the Palaeocene/Eocene boundary. *Nature*, 358:319–322.
- Meisel, T., Schoener, N., Paliulionyte, V., and Kahr, E., 2002. Determination of rare earth elements, Y, Th, Zr, Hf, Nb and Ta in geological reference materials G-2, G-3, SCo-1 and WGB-1 by sodium peroxide sintering and inductively coupled plasma-mass spectrometry. *Geostand. Newslett.*, 26(1):53–61.
- Norris, R.D., and Röhl, U., 1999. Carbon cycling and chronology of climate warming during the Palaeocene/Eocene transition. *Nature*, 401:775–778.
- Rea, D.K., Zachos, J.C., Owen, R.M., and Gingerich, P.D., 1990. Global change at the Paleocene-Eocene boundary: climatic and evolutionary consequences of tectonic events. *Palaeogeogr., Palaeoclimatol., Palaeoecol.*, 79:117–128.
- Shipboard Scientific Party, 2002. Leg 199 summary. In Lyle, M., Wilson, P.A., Janecek, T.R., et al., *Proc. ODP, Init. Repts.*, 199: College Station TX (Ocean Drilling Program), 1–87.
- Sulcek, Z., and Povondra, P., 1989. *Methods of Decomposition in Inorganic Analysis*: Boca Raton, FL (CRC Press).
- Zachos, J.C., Lohmann, K.C., Walker, J.C.G., and Wise, S.W., Jr., 1993. Abrupt climate changes and transient climates during the Paleogene: a marine perspective. *J. Geol.*, 101:191–213.

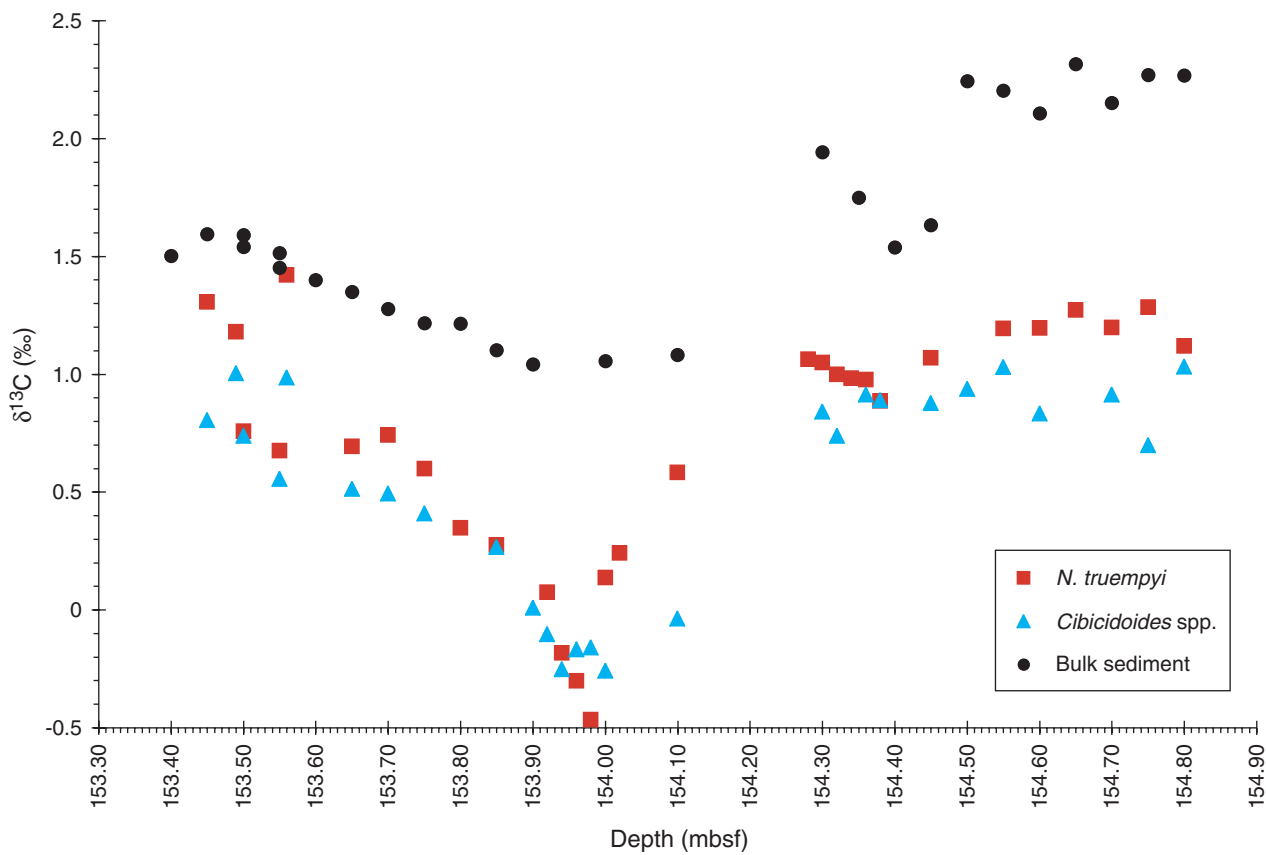
Figure F1. $\delta^{13}\text{C}$ values from R. Norris (pers. comm., 2003).

Figure F2. A. Downcore profiles of elemental concentrations. Gray symbols are inductively coupled plasma–mass spectroscopy analyses for elements analyzed using both techniques. La plotted as representative of all rare earth elements' concentration profiles, except Ce. (Continued on next page.)

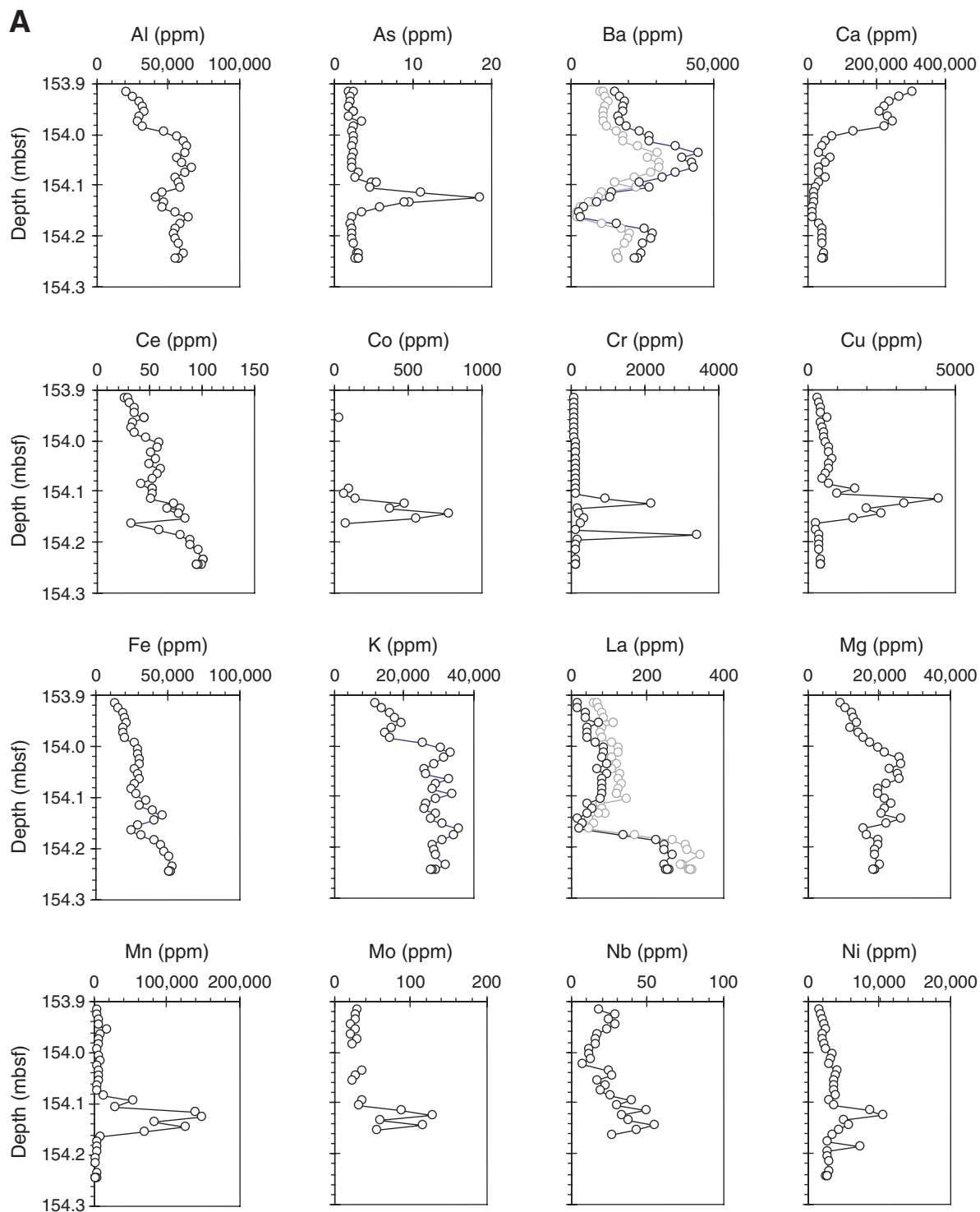


Figure F2 (continued). B. Downcore profiles of elemental concentrations.

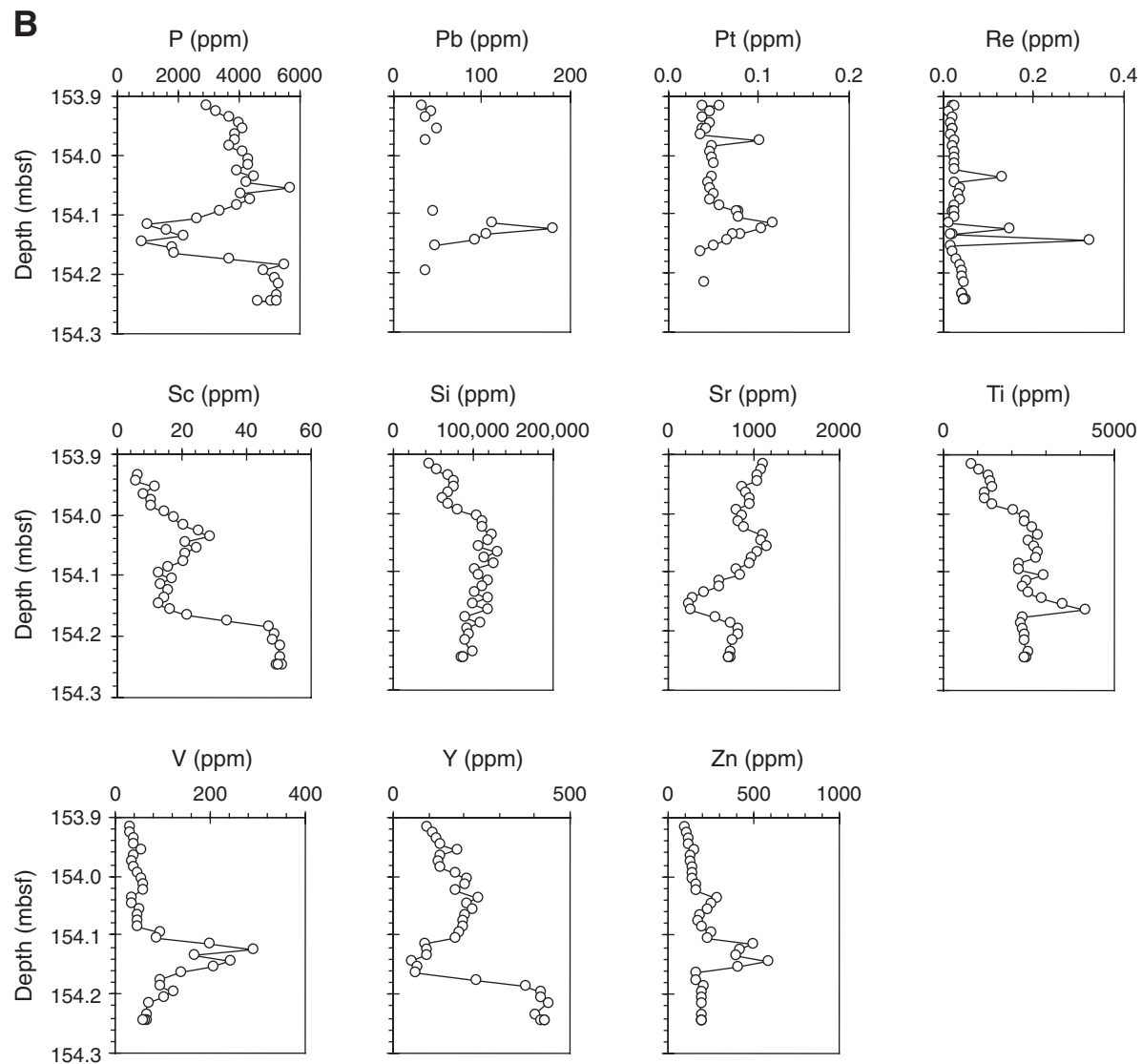


Figure F3. Post-Archean Australian Shale-normalized rare earth element patterns. Sample identifications in legend are meters below seafloor.

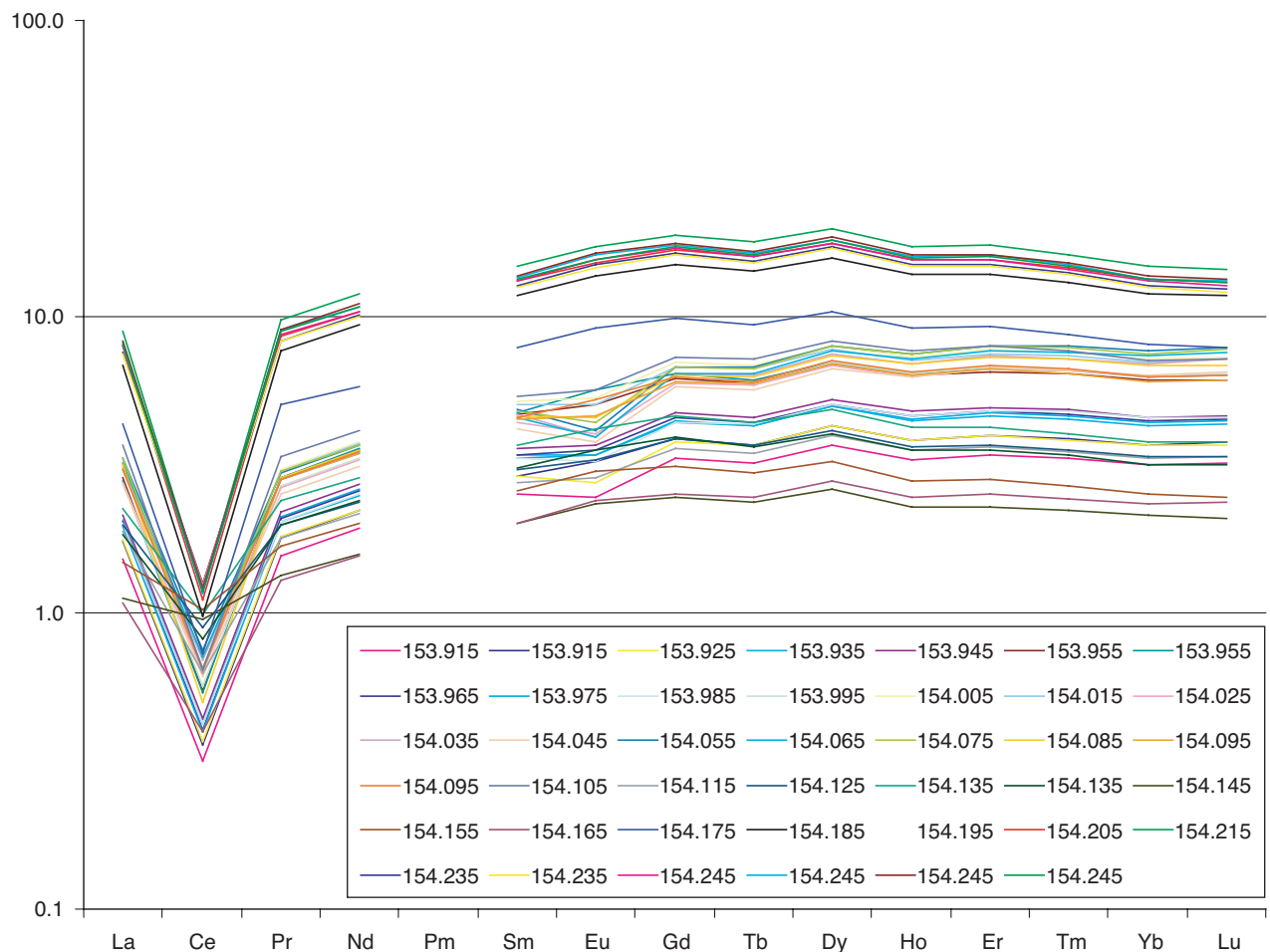


Table T1. Elemental concentrations determined by inductively coupled plasma-optical emission spectrometer. (Continued on next page.)

Core, section, interval (cm)	Depth (mbsf)	Elemental concentration (ppm)											
		Al	Ba	Ca	Fe	K	Mg	Mn	P	Si	Sr	Ti	Cd
199-1221C-													
11X-3, 51–52	153.915	19,841	14,938	302,246	12,934	11,220	8,586	2,508	2,898	42,905	1,080	799	BDL
11X-3, 52–53	153.925	23,772	16,638	260,223	15,201	12,988	10,024	3,283	3,200	53,561	1,068	1,024	BDL
11X-3, 53–54	153.935	28,680	18,525	233,793	18,508	15,658	11,996	4,249	3,643	66,349	1,025	1,296	BDL
11X-3, 54–55	153.945	31,085	18,009	221,205	19,396	17,006	12,365	5,036	3,917	74,838	1,011	1,326	BDL
11X-3, 55–56	153.955	32,685	17,641	205,733	20,678	19,000	13,229	15,415	4,050	74,138	838	1,368	BDL
11X-3, 56–57	153.965	28,423	16,219	229,984	17,771	16,132	11,371	5,776	3,841	66,418	896	1,150	BDL
11X-3, 57–58	153.975	27,547	16,825	241,685	17,717	13,938	13,665	4,248	3,831	60,671	940	1,191	BDL
11X-3, 58–59	153.985	31,331	18,735	218,177	19,743	15,551	15,148	3,635	3,653	67,336	944	1,374	BDL
11X-3, 59–60	153.995	46,200	23,357	126,385	26,057	25,070	16,925	3,207	4,060	79,385	789	1,975	BDL
11X-3, 60–61	154.005	55,162	26,888	66,946	28,909	30,098	19,182	4,835	4,237	102,755	845	2,318	BDL
11X-3, 61–62	154.015	59,856	26,801	47,024	28,012	32,711	21,125	6,926	4,258	109,204	793	2,361	BDL
11X-3, 62–63	154.025	62,331	36,031	35,733	29,630	30,931	25,167	2,949	3,867	109,491	876	2,554	BDL
11X-3, 63–64	154.035	61,376	44,201	29,590	29,969	28,181	25,909	5,235	4,436	122,592	1,082	2,714	8.66
11X-3, 64–65	154.045	55,647	38,372	61,754	26,620	25,273	22,309	4,462	4,208	117,541	1,076	2,445	6.13
11X-3, 65–66	154.055	58,155	41,900	46,172	28,230	25,773	24,607	5,476	5,616	104,301	1,140	2,634	3.96
11X-3, 66–67	154.065	66,011	42,466	27,400	29,525	32,268	25,126	2,465	4,022	128,436	1,014	2,720	2.83
11X-3, 67–68	154.075	60,730	36,109	26,392	25,792	28,676	21,568	2,614	4,295	111,544	952	2,678	BDL
11X-3, 68–69	154.085	54,285	31,327	48,974	23,391	27,975	19,213	10,610	3,877	124,291	942	2,185	BDL
11X-3, 69–70	154.095	56,322	23,572	29,340	26,950	33,326	19,167	52,527	3,295	99,613	786	2,167	BDL
11X-3, 70–71	154.105	57,494	27,189	20,246	34,019	28,884	21,044	27,620	2,587	104,103	815	2,886	BDL
11X-3, 71–72	154.115	44,949	13,802	12,097	29,422	25,674	22,836	138,035	937	116,234	573	2,393	4.13
11X-3, 72–73	154.125	40,578	13,040	14,216	39,189	25,215	21,150	146,403	1,569	110,072	588	2,267	BDL
11X-3, 73–74	154.135	46,534	8,371	15,793	45,719	28,854	20,131	80,536	2,097	99,866	409	2,467	BDL
11X-3, 74–75	154.145	44,629	4,145	7,554	39,739	27,307	25,651	123,497	723	115,563	274	2,818	BDL
11X-3, 75–76	154.155	53,713	2,172	9,498	28,738	30,364	21,477	68,053	1,778	97,579	231	3,445	BDL
11X-3, 76–77	154.165	62,672	2,588	10,553	23,860	35,305	15,323	6,331	1,784	117,819	234	4,119	BDL
11X-3, 77–78	154.175	57,174	15,562	30,937	30,307	33,893	15,993	2,635	3,607	88,724	541	2,296	BDL
11X-3, 78–79	154.185	54,382	25,244	36,869	40,073	30,534	19,168	1,289	5,424	107,311	719	2,238	BDL
11X-3, 79–80	154.195	52,678	28,303	35,948	44,761	27,794	19,118	1,685	4,764	89,586	795	2,303	BDL
11X-3, 80–81	154.205	54,370	27,347	36,818	46,258	28,261	18,514	1,037	5,106	92,769	791	2,337	BDL
11X-3, 81–82	154.215	56,650	24,435	37,943	49,835	28,675	18,484	769	5,236	88,164	731	2,331	BDL
11X-3, 83–84	154.235	59,693	24,148	40,870	52,406	31,405	19,589	2,898	5,208	97,960	704	2,457	BDL
11X-3, 84–85	154.245	56,183	23,246	40,845	50,558	28,612	18,541	2,205	4,975	86,692	710	2,379	BDL
11X-3, 85–86	154.245	55,949	22,782	36,245	50,654	27,985	18,241	967	4,575	84,045	696	2,347	BDL
11X-3, 86–87	154.245	54,364	22,098	35,868	50,312	27,312	17,883	717	5,200	85,819	686	2,337	BDL

Note: BDL = below detection limit.

Table T1 (continued).

Core, section, interval (cm)	Depth (mbsf)	Elemental concentration (ppm)											
		Co	Cr	Cu	La	Mo	Nb	Ni	Pb	Sc	V	Y	Zn
199-1221C-													
11X-3, 51–52	153.915	BDL	50.6	275.7	12.3	28.3	17.2	1,293	31	BDL	29.3	90.5	92.9
11X-3, 52–53	153.925	BDL	54.9	313.4	14.6	25.0	27.7	1,510	40	BDL	28.9	104.9	99.7
11X-3, 53–54	153.935	BDL	49.9	361.6	34.8	25.2	23.3	1,923	35	6.1	35.3	117.4	109.7
11X-3, 54–55	153.945	BDL	60.1	396.2	35.0	19.3	28.4	2,153	BDL	5.2	37.0	131.4	113.3
11X-3, 55–56	153.955	23.8	55.4	592.0	70.3	24.8	23.0	2,331	46	11.5	53.3	177.7	139.5
11X-3, 56–57	153.965	BDL	47.3	388.6	38.7	20.2	16.5	1,803	BDL	7.5	35.2	127.9	118.5
11X-3, 57–58	153.975	BDL	50.4	446.8	38.9	28.0	15.3	1,875	35	9.8	32.9	125.0	125.6
11X-3, 58–59	153.985	BDL	56.1	482.5	37.0	21.5	14.7	2,003	BDL	9.7	35.1	127.0	136.5
11X-3, 59–60	153.995	BDL	65.6	478.7	62.3	BDL	11.2	2,323	BDL	14.4	44.4	171.5	137.1
11X-3, 60–61	154.005	BDL	70.6	540.9	80.0	BDL	11.0	3,135	BDL	17.1	51.2	202.1	134.7
11X-3, 61–62	154.015	BDL	69.1	642.1	82.2	BDL	11.8	3,094	BDL	20.2	57.6	198.8	160.2
11X-3, 62–63	154.025	BDL	83.2	667.9	76.6	BDL	6.7	2,869	BDL	24.9	55.7	173.2	160.7
11X-3, 63–64	154.035	BDL	91.9	795.1	89.2	34.6	23.8	3,990	BDL	28.5	31.3	237.9	278.0
11X-3, 64–65	154.045	BDL	81.9	677.8	65.5	25.1	25.6	3,696	BDL	20.6	32.4	202.8	240.8
11X-3, 65–66	154.055	BDL	78.8	675.5	90.3	20.7	16.1	3,491	BDL	24.4	48.2	218.6	223.6
11X-3, 66–67	154.065	BDL	89.2	538.2	75.6	BDL	21.8	3,516	BDL	20.7	46.0	197.2	182.1
11X-3, 67–68	154.075	BDL	81.9	465.9	79.0	BDL	18.7	3,509	BDL	20.2	45.4	195.8	169.5
11X-3, 68–69	154.085	BDL	73.4	666.3	76.6	BDL	24.5	3,786	BDL	15.2	45.0	192.4	187.5
11X-3, 69–70	154.095	86.9	77.0	1,572.8	75.3	34.3	39.2	2,784	44	12.4	90.0	182.0	244.9
11X-3, 70–71	154.105	50.5	94.0	947.3	75.0	30.1	28.8	3,400	BDL	16.5	83.6	173.9	226.7
11X-3, 71–72	154.115	133.5	879.1	4,394.0	38.3	86.5	48.0	8,524	109	12.9	194.8	88.4	492.2
11X-3, 72–73	154.125	466.1	2,118.9	3,246.5	50.1	125.9	32.6	10,257	179	15.0	289.3	90.7	414.8
11X-3, 73–74	154.135	367.7	134.3	1,927.7	39.3	59.0	36.2	4,863	104	14.0	164.4	90.0	385.6
11X-3, 74–75	154.145	764.3	174.3	2,418.2	11.8	113.2	53.5	5,494	90	12.6	239.6	48.6	577.1
11X-3, 75–76	154.155	543.4	304.8	1,478.6	24.8	53.7	41.7	4,051	45	15.8	203.4	66.7	398.6
11X-3, 76–77	154.165	65.5	203.4	233.8	16.3	BDL	25.9	3,289	BDL	21.2	135.8	60.1	151.7
11X-3, 77–78	154.175	BDL	102.3	245.2	134.2	BDL	BDL	2,475	BDL	33.6	91.9	232.7	152.4
11X-3, 78–79	154.185	BDL	3,359.2	310.5	219.0	BDL	BDL	7,091	BDL	46.5	92.1	370.0	200.4
11X-3, 79–80	154.195	BDL	143.9	329.4	240.3	BDL	BDL	2,490	34	48.4	120.7	411.3	185.4
11X-3, 80–81	154.205	BDL	108.2	318.7	242.7	BDL	BDL	2,459	BDL	47.4	99.6	416.3	188.5
11X-3, 81–82	154.215	BDL	104.8	339.3	260.9	BDL	BDL	2,675	BDL	50.0	66.3	438.0	186.8
11X-3, 83–84	154.235	BDL	102.3	379.4	239.3	BDL	BDL	2,740	BDL	50.2	65.2	397.9	187.9
11X-3, 84–85	154.245	BDL	101.7	377.3	246.6	BDL	BDL	2,396	BDL	49.1	62.9	414.3	189.7
11X-3, 85–86	154.245	BDL	103.3	374.6	254.5	BDL	BDL	2,566	BDL	50.5	61.4	426.4	191.6
11X-3, 86–87	154.245	BDL	98.7	365.3	249.4	BDL	BDL	2,497	BDL	49.5	57.9	424.3	185.8

Table T2. Elemental concentrations determined by inductively coupled plasma–mass spectroscopy.

Core, section, interval (cm)	Depth (mbsf)	Elemental concentrations (ppm)																	
		As	Ba	La	Ce	Pr	Nd	Sm	Eu	Gd	Tb	Dy	Ho	Er	Tm	Yb	Lu	Re	Pt
199-1221C-																			
11X-3, 51–52	153.915	1.61	9,604	57.48	25.17	13.89	61.64	14.04	2.70	15.56	2.46	16.17	3.29	9.93	1.33	8.85	1.37	0.02	0.04
11X-3, 51–52	153.915	2.37	11,059	66.26	28.63	15.90	71.06	16.22	3.55	18.27	2.84	18.74	3.84	11.53	1.55	10.31	1.62	0.02	0.05
11X-3, 52–53	153.925	1.92	11,235	67.18	29.27	16.08	71.29	16.31	3.01	17.76	2.85	18.76	3.85	11.55	1.54	10.26	1.59	0.01	0.04
11X-3, 53–54	153.935	1.97	12,423	78.13	33.79	18.75	83.19	19.09	3.73	20.92	3.30	21.81	4.47	13.45	1.80	11.94	1.86	0.02	0.04
11X-3, 54–55	153.945	1.73	11,650	81.46	35.03	19.58	87.08	20.19	4.04	22.35	3.52	23.09	4.77	14.33	1.94	12.78	1.98	0.01	0.04
11X-3, 55–56	153.955	2.25	10,992	107.99	43.50	25.43	112.84	26.22	5.57	29.03	4.60	30.49	6.32	18.95	2.57	16.99	2.64	0.02	0.04
11X-3, 55–56	153.955	2.36	10,981	106.47	43.00	25.55	114.66	26.57	6.21	30.24	4.71	30.90	6.39	19.45	2.63	17.49	2.72	0.02	0.04
11X-3, 56–57	153.965	1.72	10,661	77.43	32.20	18.58	82.76	19.09	3.87	21.32	3.37	22.31	4.63	13.92	1.88	12.49	1.95	0.01	0.03
11X-3, 57–58	153.975	3.39	10,740	74.72	31.76	18.03	79.87	18.63	3.74	20.69	3.30	21.89	4.53	13.68	1.84	12.25	1.91	0.02	0.10
11X-3, 58–59	153.985	2.34	12,331	76.40	33.91	18.05	80.42	18.61	3.58	20.78	3.33	22.21	4.59	13.99	1.91	12.78	1.97	0.02	0.05
11X-3, 59–60	153.995	2.17	15,505	104.24	45.51	23.82	106.48	25.13	5.10	28.50	4.54	30.72	6.44	19.49	2.63	17.53	2.75	0.02	0.04
11X-3, 60–61	154.005	2.25	17,637	121.51	57.13	27.25	121.49	28.84	5.85	32.93	5.26	35.19	7.32	22.56	3.04	20.25	3.14	0.02	0.05
11X-3, 61–62	154.015	2.35	17,548	120.04	56.19	26.65	119.78	28.20	5.57	31.61	5.14	34.27	7.11	21.73	2.95	19.75	3.08	0.02	0.05
11X-3, 62–63	154.025	2.13	23,169	104.94	50.48	23.46	104.80	24.74	4.41	28.10	4.52	30.08	6.29	19.23	2.62	17.53	2.74	0.02	BDL
11X-3, 63–64	154.035	2.39	29,731	115.66	55.17	25.17	111.80	26.25	4.33	30.10	4.89	32.75	6.91	21.38	2.89	19.49	3.10	0.12	0.05
11X-3, 64–65	154.045	2.19	26,236	102.94	48.77	22.55	100.29	23.40	4.15	27.19	4.36	29.45	6.26	19.38	2.65	17.82	2.80	0.02	0.04
11X-3, 65–66	154.055	2.01	30,338	126.38	59.93	26.50	117.16	27.17	4.54	31.83	5.19	35.12	7.45	23.09	3.17	21.59	3.39	0.04	0.04
11X-3, 66–67	154.065	2.10	30,224	122.37	57.01	25.06	111.08	25.52	4.30	30.03	4.92	33.66	7.20	22.23	3.04	20.60	3.27	0.03	0.05
11X-3, 67–68	154.075	2.92	27,798	126.91	52.01	26.66	117.23	26.88	4.86	31.55	5.11	34.87	7.44	23.10	3.15	21.01	3.32	0.03	0.04
11X-3, 68–69	154.085	2.51	21,840	120.32	39.89	25.53	112.85	25.89	5.02	29.68	4.79	32.59	6.91	21.21	2.86	19.08	2.95	0.02	0.05
11X-3, 69–70	154.095	4.63	15,146	117.05	51.84	25.05	110.56	25.10	5.09	28.40	4.56	30.65	6.35	19.23	2.58	16.97	2.64	0.02	0.07
11X-3, 69–70	154.095	5.28	15,000	114.98	51.15	25.22	111.65	25.40	5.78	29.53	4.64	31.13	6.49	19.73	2.66	17.53	2.72	0.02	0.07
11X-3, 70–71	154.105	4.34	22,620	140.04	51.12	30.11	132.26	30.11	6.26	34.27	5.55	36.51	7.64	23.13	3.06	19.91	3.08	0.02	0.08
11X-3, 71–72	154.115	10.76	10,136	71.20	49.80	15.96	69.43	15.34	3.13	16.77	2.65	17.49	3.55	10.56	1.39	9.31	1.46	0.01	0.11
11X-3, 72–73	154.125	18.27	9,063	75.41	71.48	17.54	75.82	16.96	3.63	18.27	2.83	18.11	3.63	10.67	1.42	9.42	1.45	0.14	0.10
11X-3, 73–74	154.135	9.32	6,881	85.04	78.67	21.32	91.91	20.62	4.58	21.62	3.37	21.36	4.22	12.28	1.62	10.53	1.62	0.02	0.08
11X-3, 73–74	154.135	8.82	5,718	69.95	65.22	17.70	76.98	17.28	3.88	18.39	2.79	17.79	3.53	10.31	1.36	8.90	1.36	0.01	0.07
11X-3, 74–75	154.145	5.65	2,993	42.74	76.48	11.84	50.56	11.30	2.56	11.53	1.82	11.52	2.27	6.61	0.89	5.96	0.90	0.32	0.06
11X-3, 75–76	154.155	3.37	1,481	56.25	82.44	14.93	64.24	14.48	3.30	14.62	2.28	14.31	2.80	8.22	1.07	7.04	1.06	0.01	0.05
11X-3, 76–77	154.165	2.05	1,723	41.11	31.59	11.43	49.90	11.28	2.64	11.85	1.88	12.23	2.46	7.31	0.97	6.53	1.01	0.02	0.03
11X-3, 77–78	154.175	1.97	10,364	164.40	57.95	44.78	186.03	43.80	10.08	46.62	7.25	45.89	9.15	26.80	3.48	22.55	3.39	0.02	BDL
11X-3, 78–79	154.185	2.14	17,083	260.86	77.84	68.41	301.52	66.31	15.14	70.79	10.91	69.32	13.81	40.24	5.25	33.52	5.07	0.03	BDL
11X-3, 9–80	154.195	2.09	20,012	295.33	87.58	75.84	328.89	72.89	16.31	77.78	11.97	76.22	15.30	44.37	5.78	37.02	5.54	0.04	BDL
11X-3, 80–81	154.205	2.14	19,327	301.71	87.97	76.88	334.48	73.79	16.79	79.07	12.26	77.84	15.52	45.43	5.86	37.36	5.58	0.04	BDL
11X-3, 81–82	154.215	2.28	18,274	337.45	95.59	87.11	380.67	82.69	19.06	88.96	13.79	87.67	17.32	50.64	6.50	41.24	6.19	0.04	0.04
11X-3, 83–84	154.235	2.70	15,747	288.32	99.97	73.79	325.05	71.36	16.51	77.37	11.89	75.78	15.06	43.33	5.60	35.63	5.32	0.04	BDL
11X-3, 83–84	154.235	2.92	15,601	283.42	99.35	73.81	320.62	70.58	16.18	75.78	11.69	74.52	14.77	42.94	5.54	35.00	5.22	0.04	BDL
11X-3, 84–85	154.245	2.61	15,911	303.68	98.10	77.10	333.47	73.68	17.13	79.57	12.22	77.72	15.53	45.03	5.78	36.76	5.46	0.04	BDL
11X-3, 85–86	154.255	2.57	16,305	311.16	93.23	80.16	346.92	76.10	17.72	82.25	12.66	80.03	16.01	46.64	5.96	37.66	5.66	0.04	BDL
11X-3, 86–87	154.265	2.94	16,186	314.53	95.67	80.00	353.45	76.58	17.92	83.49	12.85	81.31	16.20	47.10	6.08	38.52	5.74	0.04	BDL
11X-3, 86–87	154.265	2.83	15,944	307.57	94.37	79.32	344.74	75.34	17.19	81.35	12.50	79.69	15.86	46.07	5.95	37.51	5.62	0.04	BDL

Note: BDL = below detection limit.

Table T3. Correlation analysis of elemental data.

	Al	As	Ba*	Ba†	Ca	Ce	Co	Cr	Cu	Fe	K	La1	La2	Mg	Mn	Mo	Nb	Ni	P	Pb	Pt	Re	Sc	Si	Sr	Ti	V	Y	Zn	
Al	1.00																													
As	-0.09	1.00																												
Ba*	0.48	-0.33	1.00																											
Ba†	0.50	-0.30	0.99	1.00																										
Ca	-0.89	-0.30	-0.19	-0.23	1.00																									
Ce	0.53	0.13	0.05	0.08	-0.64	1.00																								
Co	-0.21	0.30	-0.62	-0.58	-0.41	0.89	1.00																							
Cr	0.02	0.45	-0.11	-0.11	-0.21	0.19	0.25	1.00																						
Cu	-0.04	0.86	-0.33	-0.30	-0.34	0.06	0.36	0.32	1.00																					
Fe	0.55	0.21	0.06	0.1	-0.67	0.95	0.62	0.19	0.10	1.00																				
K	0.94	0.07	0.21	0.22	-0.93	0.55	-0.03	0.13	0.11	0.57	1.00																			
La1	0.45	-0.21	0.30	0.31	-0.39	0.81	-0.63	0.13	-0.33	0.81	0.39	1.00																		
La2	0.42	-0.23	0.30	0.32	-0.35	0.79	-0.60	0.10	-0.35	0.80	0.34	0.99	1.00																	
Mg	0.76	0.27	0.45	0.47	-0.83	0.44	0.70	0.13	0.41	0.44	0.69	0.14	0.10	1.00																
Mn	-0.10	0.88	-0.49	-0.46	-0.32	0.11	0.63	0.34	0.96	0.13	0.10	-0.35	-0.37	0.34	1.00															
Mo	0.18	0.85	-0.47	-0.44	-0.58	0.67	0.71	0.77	0.87	0.70	0.42	-0.25	-0.44	0.51	0.95	1.00														
Nb	-0.01	0.52	-0.51	-0.46	-0.37	0.46	0.65	0.35	0.73	0.44	0.18	-0.43	-0.42	0.24	0.79	0.72	1.00													
Ni	0.19	0.82	-0.14	-0.11	-0.52	0.22	0.40	0.74	0.81	0.25	0.31	-0.10	-0.15	0.52	0.79	0.88	0.56	1.00												
P	0.26	-0.60	0.67	0.64	0.05	0.31	-0.64	-0.07	-0.72	0.27	0.06	0.69	0.69	-0.04	-0.79	-0.82	-0.78	-0.46	1.00											
Pb	0.25	0.97	-0.37	-0.33	-0.58	0.40	0.30	0.88	0.83	0.57	0.37	-0.17	-0.25	0.59	0.88	0.89	0.46	0.95	-0.25	1.00										
Pt	-0.05	0.78	-0.22	-0.19	-0.27	0.16	0.08	0.61	0.79	0.29	0.07	-0.19	-0.16	0.28	0.73	0.63	0.48	0.68	-0.54	0.64	1.00									
Re	0.05	0.35	-0.14	-0.13	-0.29	0.29	0.76	0.16	0.38	0.29	0.12	-0.04	-0.06	0.42	0.51	0.70	0.46	0.41	-0.33	0.45	0.20	1.00								
Sc	0.54	-0.23	0.25	0.26	-0.47	0.83	-0.15	0.15	-0.35	0.83	0.46	0.96	0.94	0.16	-0.35	0.05	-0.24	-0.10	0.60	-0.15	-0.22	0.02	1.00							
Si	0.80	0.26	0.36	0.38	-0.85	0.27	0.29	0.22	0.37	0.31	0.79	0.05	0.00	0.87	0.31	0.53	0.27	0.58	-0.13	0.68	0.19	0.30	0.06	1.00						
Sr	-0.25	-0.38	0.71	0.68	0.53	-0.43	-0.63	-0.21	-0.42	-0.43	-0.50	-0.05	-0.02	-0.20	-0.55	-0.74	-0.61	-0.40	0.54	-0.51	-0.28	-0.32	-0.11	-0.28	1.00					
Ti	0.84	0.12	0.06	0.1	-0.88	0.43	0.17	0.08	0.20	0.45	0.85	0.16	0.12	0.71	0.22	0.45	0.30	0.37	-0.18	0.41	0.05	0.22	0.27	0.80	-0.59	1.00				
V	0.10	0.78	-0.56	-0.52	-0.51	0.35	0.80	0.43	0.78	0.34	0.32	-0.12	-0.15	0.36	0.88	0.94	0.74	0.76	-0.69	0.82	0.57	0.53	-0.08	0.37	-0.78	0.46	1.00			
Y	0.45	-0.31	0.43	0.43	-0.32	0.74	-0.68	0.07	-0.42	0.74	0.34	0.98	0.98	0.13	-0.46	-0.56	-0.55	-0.19	0.79	-0.35	-0.30	-0.09	0.93	0.03	0.10	0.10	-0.26	1.00		
Zn	0.18	0.69	-0.31	-0.27	-0.56	0.35	0.80	0.28	0.86	0.34	0.31	-0.16	-0.19	0.61	0.89	0.87	0.82	0.76	-0.63	0.71	0.58	0.63	-0.13	0.52	-0.60	0.46	0.84	-0.25	1.00	

Notes: Correlation of values between Tables **T1**, p. 9, and **T2**, p. 11. Values greater than 0.90 or less than -0.90 are in bold type. * = analyzed by inductively coupled plasma-optical emission spectrometer. † = analyzed by inductively coupled plasma-mass spectroscopy.